

# Toward a structural understanding of turbulent drag reduction: nonlinear coherent states in viscoelastic shear flows

Philip A. Stone,<sup>1</sup> Fabian Waleffe,<sup>2</sup> and Michael D. Graham<sup>1,\*</sup>

<sup>1</sup>*Department of Chemical Engineering*

<sup>2</sup>*Departments of Mathematics and Engineering Physics,  
University of Wisconsin-Madison, Madison, WI 53706.*

(Dated: October 26, 2018)

Nontrivial steady flows have recently been found that capture the main structures of the turbulent buffer layer. We study the effects of polymer addition on these “exact coherent states” (ECS) in plane Couette flow. Despite the simplicity of the ECS flows, these effects closely mirror those observed experimentally: structures shift to larger length scales, wall-normal fluctuations are suppressed while streamwise ones are enhanced, and drag is reduced. The mechanism underlying these effects is elucidated. These results suggest that the ECS are closely related to buffer layer turbulence.

PACS numbers: 83.60.Yz,83.80.Rs,47.20.Ky,47.27.Cn

Rheological drag reduction, the suppression by additives of skin friction in turbulent flow, has received much attention since its discovery in 1947 [1, 2, 3]. For many polymer-solvent systems, the pressure drop measured in the pipe flow of the solution can be 30 – 50% less than for the solvent alone. The central rheological feature of drag-reducing additives is their extensional behavior in solution: for dilute polymer solutions in particular the stresses arising in extensional flow can be orders of magnitude larger than those developed in a shear flow. This fact is well-recognized; nevertheless the mechanism of interaction between polymer stretching and turbulent structure is not well-understood and the goal of the present work is to attempt to shed light on this interaction.

A key structural observation from experiments and direct numerical simulations (DNS) of drag-reducing solutions is the modification of the buffer region near the wall [4, 5, 6, 7, 8, 9, 10]. It has long been known that the flow in this region is very structured, containing streamwise vortices that lead to streaks in the streamwise velocity [11]; these structures are thickened in both the wall-normal and spanwise directions during flow of drag reducing solutions [4, 5]. Because of its importance in the production and dissipation of turbulent energy [11], any effort to mechanistically understand rheological drag reduction should address this region.

To better understand the effect of the polymer on the buffer layer, we wish to study a model flow that has structures similar to those seen in this region but without the full complexities of time-dependent turbulent flows. Fortunately, a family of such flows exists, in the recently-discovered “exact coherent states” (ECS) found by computational bifurcation analysis in plane Couette and plane Poiseuille flows [12, 13, 14, 15, 16]. These are three-dimensional, traveling wave flows (hence steady in a traveling reference frame) that appear via saddle-node bifurcations [35] at a Reynolds number somewhat below the transition value seen in experiments [17, 18]. The

structure of the ECS captures the counter-rotating staggered streamwise vortices that dominate the structure in the buffer region. From the dynamical point of view, there is evidence that these states form a part of the dynamical skeleton of the turbulent flow: i.e., they are saddle points that underlie the strange attractor of turbulence [19, 20]. Finally, the nonlinear self-sustaining mechanism underlying these states has been elucidated [21]. A perturbation of the base flow in the form of streamwise vortices redistributes the streamwise momentum of the flow. This redistribution creates spanwise fluctuations in the streamwise velocity, the “streaks”. The spanwise inflections in the streamwise velocity profile lead to a three-dimensional instability that develops into staggered nearly-streamwise vortices that regenerate the streaks. Because the ECS capture the structures of the buffer region and are mechanistically well-understood, we believe that they provide an excellent simplified, yet still exact, model flow for studying polymer drag reduction. The leading order effect of viscoelasticity on the ECS is therefore the focus of the present study.

To begin, we briefly describe a general result relating polymer stretch to flow kinematics. For a trajectory in a flow field, the Liapunov exponents give the Lagrangian time-averaged rate of stretch of material lines. If the largest Liapunov exponent,  $\sigma_{max}$ , is positive, the flow is extensional on average. In particular, for homogeneous turbulence, the expected value of  $\sigma_{max}$  is positive [22] and we show below that this is also the case for the ECS. Now consider the dynamics of a Hookean dumbbell model of a polymer in a flow field. The end-to-end vector  $\mathbf{q}$  of the dumbbell evolves in the flow field,  $\mathbf{v}$ , as:

$$\frac{D\mathbf{q}}{Dt} = \mathbf{q} \cdot \nabla \mathbf{v} - \frac{1}{2\lambda} \mathbf{q} + \boldsymbol{\xi}(t), \quad (1)$$

where  $D/Dt$  is the time derivative evaluated on a fluid element,  $\lambda$  is the stress relaxation time for the dumbbell and  $\boldsymbol{\xi}(t)$  is the random Brownian force. Noting that an infinitesimal material line satisfies the same expression

but with  $\lambda^{-1}$  and  $\xi$  set to zero, it is straightforward to show that Hookean dumbbells will stretch indefinitely in a flow if and only if  $\lambda\sigma_{max} \equiv We_\sigma > \frac{1}{2}$ , where  $We_\sigma$  is a Weissenberg number based on  $\sigma_{max}$ . This result is a specific statement of an idea that originated with Lumley [23] (see also [24, 25, 26, 27]). The computations below show the importance of  $We_\sigma$  in determining the effect of polymers on coherent structures.

We study here the effect of polymer on the exact coherent states that arise in a variant of plane Couette flow [14]. Denoting the streamwise direction as  $x$ , the wall-normal direction as  $y$ , and the spanwise, or vorticity, direction as  $z$ , we consider a flow with boundary conditions  $\frac{\partial v_x}{\partial y} = 1, v_y = \frac{\partial v_z}{\partial y} = 0$  at  $y = \pm 1$ . The characteristic velocity,  $U$ , and the half-height of the channel,  $l$ , have been used to scale the velocity and positions, respectively. These ‘‘constant vorticity’’ boundary conditions provide an advantage over no-slip conditions in that they allow us to model only the buffer region in our domain by eliminating the viscous sublayer. (Exact coherent states found using no-slip BCs [16] show a qualitatively identical vortical structure, only offset from the wall by a small region comprising the viscous sublayer.) Periodic boundary conditions are applied in the streamwise and spanwise directions. For this study, the wavelength of the structures in the streamwise and spanwise directions are fixed at  $\ell_x = 2\pi/0.40$  and  $\ell_z = 2\pi/1.0$ , respectively (or 165 and 66, if expressed in wall units at a Reynolds number of 110). For this flow, a trivial (Couette) base state exists,  $v_x(y) = y$ ; the maximum mean velocity for the ECS is significantly reduced compared to the base state velocity due to the enhanced transport of momentum [14].

In our formulation, time,  $t$ , is scaled with  $l/U$ , and pressure,  $p$ , with  $\rho U^2$ , where  $\rho$  is the fluid density. The stress due to the polymer,  $\tau_p$ , is nondimensionalized with the polymer elastic modulus,  $G = \eta_p/\lambda$ , where  $\eta_p$  is the polymer contribution to the zero-shear viscosity and  $\lambda$  is the relaxation time for the polymer. The momentum and mass balances are

$$\frac{D\mathbf{v}}{Dt} = -\nabla p + \beta \frac{1}{Re} \nabla^2 \mathbf{v} + (1 - \beta) \frac{1}{Re^2} \frac{1}{El} (\nabla \cdot \tau_p), \quad (2)$$

$$\nabla \cdot \mathbf{v} = 0, \quad (3)$$

where  $\eta_s$  is the solvent viscosity,  $El = \lambda(\eta_s + \eta_p)/\rho l^2$  and  $\beta = \eta_s/(\eta_s + \eta_p)$ . The Reynolds number,  $Re$ , is based on the total viscosity,  $Re = \rho Ul/(\eta_s + \eta_p)$ .

We calculate the polymer stress with the commonly used FENE-P model [28], which idealizes the polymer molecules as bead-spring dumbbells with finitely extensible springs. With this model, the non-dimensional structure tensor  $\alpha$  ( $= \langle \mathbf{q}\mathbf{q} \rangle$ , where  $\langle \rangle$  denotes ensemble aver-

age) evolves according to:

$$\frac{\alpha}{1 - \frac{tr\alpha}{b}} + We \left( \frac{D\alpha}{Dt} - \alpha \cdot \nabla \mathbf{v} - \nabla \mathbf{v}^T \cdot \alpha \right) = \frac{b\delta}{b+2}, \quad (4)$$

$$\tau_p = \frac{b+5}{b} \left( \frac{\alpha}{1 - \frac{tr\alpha}{b}} - \left( 1 - \frac{2}{b+2} \right) \delta \right), \quad (5)$$

where  $We = \frac{\lambda U}{l}$  is the Weissenberg number based on the wall shear rate and  $b$  is proportional to the maximum extension of the dumbbell:  $tr\alpha$  cannot exceed  $b$ . A simple measure of the importance of extensional polymer stress is the magnitude of the parameter  $Ex = \frac{2}{3} \frac{b\eta_p}{\eta_s}$ . In uniaxial extension with extension rate  $\dot{\epsilon}$ ,  $Ex = 1$  implies that  $\tau_p = \tau_v$  as  $\dot{\epsilon} \rightarrow \infty$  where  $\tau_v$  is the solvent contribution to the stress. The polymer can significantly affect the flow only when  $Ex \gtrsim 1$ . In the present flow this parameter also represents the maximum ratio of polymer stress to Reynolds shear stress (the flux of  $x$ -momentum due to fluctuations in  $y$ -velocity); the scaling theory of Tabor and de Gennes [29, 30, 31] treats the regime  $Ex \gg 1$ .

The governing equations are solved through a Picard iteration. A given velocity field is first used to calculate the polymer stress tensor,  $\tau_p$ , by time-integrating Eq. 4 until a steady state is attained. For the new  $\tau_p$ , a steady state of the momentum and continuity equations is found by Newton iteration. The resulting velocity field, is used to compute the new  $\tau_p$ , and the process is repeated until the velocity field converges. Equations 2-3 are discretized as in [14], using a Fourier-Galerkin formulation with typically a  $7 \times 19 \times 7$  grid. Equation 4 is discretized with a Fourier-pseudospectral method, typically with a  $32 \times 32 \times 32$  grid, and time-integration performed with an Adams-Bashforth method. To achieve numerical stability, a small diffusive term is added to Eq. 4 (cf. [9]) and integrated with a Crank-Nicholson scheme.

Before presenting the effects of the polymer on the ECS, we recall the result that  $We_\sigma > 1/2$  implies large stretch of polymer chains. For the Newtonian ECS at  $Re = 110$  on the lower branch of the bifurcation diagram (see Fig. 1), the velocity field is very nearly ergodic, with  $\sigma_{max} \approx 0.030$ . The condition  $We_\sigma > 1/2$  thus translates into  $We \gtrsim 17$  for large polymer stretch, and for  $Ex = O(1)$ , will define the onset condition for the polymer to begin to strongly affect the flow field. In DNS of a FENE-P fluid in plane channel flow, Sureshkumar, et al. [9], found no drag reduction at  $We = 12.5$  and significant drag reduction at  $We = 25$ ; another recent DNS study [32] places the onset value at  $We \approx 20$ . This close correspondence between the onset condition predicted from the ECS kinematics and that found by DNS strongly suggests that the ECS model captures the essential structure of the buffer layer.

Fig. 1 shows how the addition of polymer stress affects the bifurcation diagram (i. e. the locus of steady state flows) for  $El = 0.20$  ( $We_\sigma \approx 2/3$ ) and  $Ex = 1$

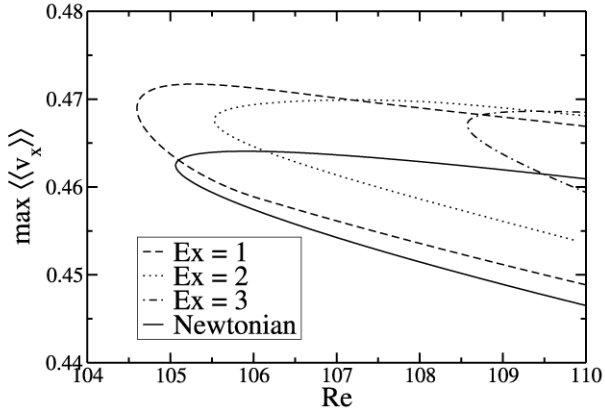


FIG. 1: Newtonian and viscoelastic ( $El = 0.20$ ,  $\beta = 0.97$ ) bifurcation diagrams. Each curve represents a locus of steady state ECS flows; the leftmost point on each curve is the position of the saddle-node bifurcation.

to 3. On the  $y$ -axis of the diagram is the maximum value of the streamwise- and spanwise-averaged streamwise velocity  $\langle\langle v_x \rangle\rangle$ . (The trivial Couette solution is at  $\max\langle\langle v_x \rangle\rangle = 1$ .) When  $Re$  attains a certain value that we denote  $Re_{sn}$ , two new steady solutions appear in a saddle-node bifurcation. For small values of  $Ex$ ,  $Re_{sn}$  decreases compared to the Newtonian value, but once the polymer stress begins to exceed the viscous ( $Ex \approx 1.5$ ),  $Re_{sn}$  increases above the Newtonian value – the presence of the polymer is suppressing the ECS. Qualitatively identical behavior is observed experimentally in the onset Reynolds number for turbulent pipe flow [7]. Note that, for a given velocity  $U$  and total viscosity  $\eta$ , the increase in critical Reynolds number corresponds to an increase in the characteristic length scale of the coherent structure, again consistent with experimental observations [4, 5, 9]. Finally, we see that  $\langle\langle v_x \rangle\rangle$  becomes larger for the viscoelastic flows than for the Newtonian – drag reduction occurs.

To examine more closely the effect of the polymer stress on the velocity fields, Fig. 2 shows results at constant  $Re$  while varying  $El$ , or, equivalently,  $We_\sigma$  (based on  $\sigma_{max} = 0.030$ ). Here we plot  $\max\langle\langle v_y'^2 \rangle\rangle$ , where the prime denotes the fluctuating part of a quantity, here wall-normal velocity. At  $Ex = 1$ , after an initial increase,  $\max\langle\langle v_y'^2 \rangle\rangle$  decreases below the Newtonian value and eventually saturates, as the polymer stress asymptotes at high  $We_\sigma$  to a fixed value relative to the viscous stress. In this case, the polymer stretch becomes nearly uniformly large throughout the domain. The decrease in wall-normal velocity with  $We_\sigma$  is even more drastic as the extensibility parameter  $Ex$  increases. Similar trends are seen in the streamwise enstrophy and Reynolds shear stress. Since  $Ex$  is related to the extensional viscosity

of the viscoelastic solution, these results show the importance of extensional stresses in affecting the ECS. The spatial maximum of  $tr\alpha$ , which is proportional to the square of the polymer extension, is also presented in Fig. 2. Finally, note that the majority of both the polymer stretch and the change in wall-normal velocity occurs in the range  $0.1 < We_\sigma < 1.0$ . In contrast to the decreases in wall normal fluctuations, streamwise enstrophy and Reynolds shear stress for  $We_\sigma \gtrsim 0.1$ , the streamwise fluctuations  $\langle\langle v_x'^2 \rangle\rangle$  are found to increase. All of these trends are observed in DNS and experiments [1, 3, 9].

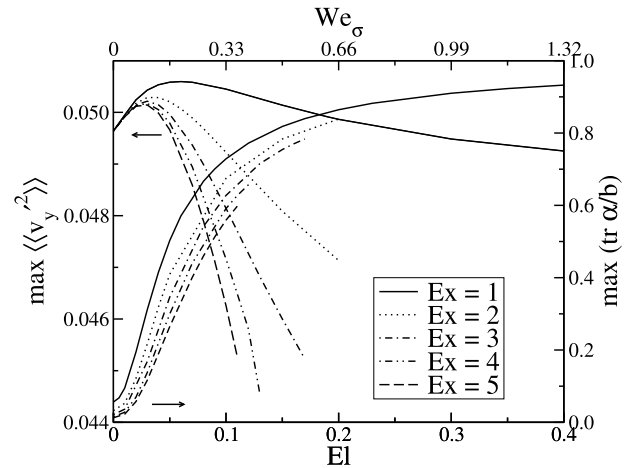


FIG. 2: Wall normal velocity and maximum polymer stretch vs.  $El$  and  $We_\sigma$ , lower branch solutions,  $Re = 110$ ,  $\beta = 0.97$ .

Turning now to how, and why, the flow structure is changed by the polymer dynamics, figures 3a-b show (a) the streamwise velocity  $v_x$  at  $y = 0.875$  (where the maximum in the polymer stress occurs) for the Newtonian lower branch solution at  $Re = 110$  and (b) the difference  $v_{x,VE} - v_{x,N}$  between the viscoelastic (VE) and Newtonian (N) solutions. Here we see the “streak” (white ribbon) and – by adding the pattern of fig. 3b to that of 3a – that this streak is “straightened out” by the viscoelasticity. Figure 3c shows a contour plot of  $f_x$ , the  $x$ -component of the force  $\mathbf{f}$  exerted by the polymer on the fluid, ( $\mathbf{f} = (1 - \beta)Re^{-2}El^{-1}\nabla \cdot \boldsymbol{\tau}_p$ ), at  $y = 0.875$ . This force is significantly negative and corresponds spatially to the region where fluid elements are leaving the streak to move into the vorticity-dominated regions. The  $y$  and  $z$  components of the force have also been examined; they are smaller than the  $x$ -component but are clearly seen to work directly against the vortex motions: e.g. where  $v_y$  is highly positive in an upwelling,  $f_y$  is highly negative. This behavior is also seen in the buffer layer structures in the DNS study of a drag-reducing polymer solution by De Angelis *et al.* [33]. The origin for this structure of the polymer force field becomes apparent on examination of polymer stresses along fluid trajectories:

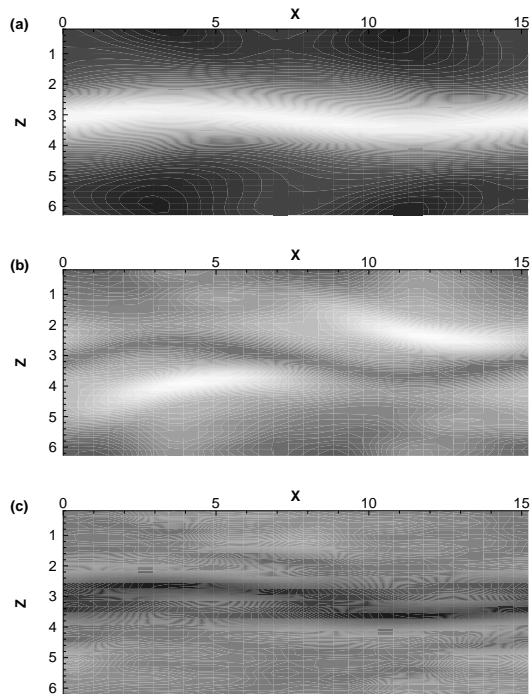


FIG. 3: Streamwise velocity for the Newtonian (N) and viscoelastic (VE) solutions and polymer force at  $y = 0.875$ . Lower branch solutions at  $Re = 110$  and for the viscoelastic solution  $El = 0.15$ ,  $Ex = 3$ , and  $\beta = 0.97$ . (a)  $v_{x,N}$  (range: 0.0 (black) — 0.889 (white)) (b)  $v_{x,VE} - v_{x,N}$  (range: -0.0395 (black) — 0.0395 (white)) (c)  $f_x$  (range: -0.00413 (black) — 0.00413 (white)). By symmetry, identical behavior with opposite signed velocity is occurring at  $y = -0.875$ .

polymer molecules stretch in (or moving into) the streak regions, remaining highly stretched until they begin to leave the streak. As molecules move from the streak into and around the vortices, they relax. The spatial gradients in stress accompanying this relaxation work against the vortices, “unwinding” them. This vortex suppression leads to collapse of the self-sustained process – or more precisely to a shift of the process to larger scales – and thus to drag reduction.

To summarize, we list several points of agreement between our results and observations from DNS and experiments in fully turbulent flow, namely: (1) the ECS bear a strong similarity to the structures observed or deduced from structural studies of the buffer layer and apparently underlie its dynamics; (2) for  $O(1)$  values of  $Ex$ , the onset Weissenberg number for drag reduction predicted from the ECS kinematics agrees closely with DNS results; (3) the effects of viscoelasticity on the Couette flow ECS are very similar to those observed in the buffer layer: (a) wall normal velocity fluctuations are suppressed and streamwise ones enhanced, (b) Reynolds shear stress decreases, (c) streamwise vorticity decreases, (d) the velocity fluctuations and polymer force are anticorrelated, and (e) drag

is reduced. Finally, at fixed  $U$  and  $\eta$  the upward shift in the onset Reynolds number corresponds to an increase in length scale for the structures, again consistent with experiments. These successes show that studying the ECS holds promise for capturing the essential physics of drag reduction. Indirectly, they also validate the view that the ECS underlie Newtonian turbulence, because the effects of polymers on the ECS so closely mirror their effects on full turbulence.

The authors gratefully acknowledge support from NSF and the donors of the Petroleum Research Fund, administered by the American Chemical Society.

\* Electronic address: graham@engr.wisc.edu

- [1] P. Virk, *AIChE J.* **21**, 225 (1975).
- [2] J. Lumley, *Annu. Rev. Fluid Mech.* **1**, 367 (1969).
- [3] W. McComb, *The Physics of Fluid Turbulence* (Oxford University Press, New York, 1990).
- [4] D. Walker and W. Tiederman, *J. Fluid Mech.* **218**, 377 (1990).
- [5] G. Donohue, W. Tiederman, and M. Reischman, *J. Fluid Mech.* **50**, 559 (1972).
- [6] J. den Toonder, M. Hulslen, G. Kuiken, and F. Nieuwstadt, *J. Fluid Mech.* **337**, 193 (1997).
- [7] A. Draad, G. Kuiken, and F. Nieuwstadt, *J. Fluid Mech.* **377**, 267 (1998).
- [8] M. Escudier, F. Presti, and S. Smith, *J. Non-Newtonian Fluid Mech.* **81**, 197 (1999).
- [9] R. Sureshkumar, A. Beris, and R. Handler, *Phys. Fluids* **9**, 743 (1997).
- [10] C. Dimitropoulos, R. Sureshkumar, A. Beris, and R. Handler, *Phys. Fluids* **13**, 1016 (2001).
- [11] S. Robinson, *Annu. Rev. Fluid Mech.* **23**, 601 (1991).
- [12] M. Nagata, *J. Fluid Mech.* **217**, 519 (1990).
- [13] R. Clever and F. Busse, *J. Fluid Mech.* **344**, 137 (1997).
- [14] F. Waleffe, *Phys. Rev. Lett.* **81**, 4140 (1998).
- [15] B. Eckhardt, K. Marzinzik, and A. Schmiegel, in *A Perspective Look at Nonlinear Media* (Springer, New York, 1998), Lecture Notes in Physics.
- [16] F. Waleffe, *J. Fluid Mech.* **435**, 93 (2001).
- [17] F. Daviaud, J. Hegseth, and P. Bergé, *Phys. Rev. Lett.* **69**, 2511 (1992).
- [18] S. Bottin, O. Dauchot, F. Daviaud, and P. Mannville, *Phys. Fluids* **10**, 2597 (1998).
- [19] J. Jimenez and M. Simens, *J. Fluid Mech.* **435**, 81 (2001).
- [20] G. Kawahara and S. Kida, *J. Fluid Mech.* **449**, 291 (2001).
- [21] F. Waleffe, *Phys. Fluids* **9**, 883 (1997).
- [22] S. Girimaji and S. Pope, *J. Fluid Mech.* **220**, 427 (1990).
- [23] J. Lumley, *Symp. Math.* **9**, 315 (1972).
- [24] G. Ryskin, *Phys. Rev. Lett.* **59**, 2059 (1987).
- [25] L. Leal, in *Structure of Turbulence and Drag Reduction* (Springer, Berlin, 1990).
- [26] M. Chertkov, *Phys. Rev. Lett.* **84**, 4761 (2000).
- [27] E. Balkovsky, A. Fouxon, and V. Lebedev, *Phys. Rev. Lett.* **84**, 4765 (2000).
- [28] R. Bird, C. Curtiss, R. Armstrong, and O. Hassager, *Dynamics of Polymeric Liquids*, vol. 2 (Wiley, New York, 1987b), 2nd ed.

- [29] M. Tabor and P. de Gennes, *Europhys. Lett.* **2**, 519 (1986).
- [30] P. de Gennes, *Introduction to Polymer Dynamics* (Cambridge University Press, New York, 1990).
- [31] K. Sreenivasan and C. White, *J. Fluid Mech.* **409**, 149 (2000).
- [32] S. Sibilla and A. Baron, *Phys. Fluids* **14**, 1123 (2002).
- [33] E. de Angelis, C. M. Casciola, and R. Piva, *Computers and Fluids* **31**, 495 (2002).
- [34] S. H. Strogatz, *Nonlinear Dynamics and Chaos: With Applications to Physics, Biology, Chemistry and Engineering* (Addison Wesley, 1994).
- [35] A saddle-node bifurcation, also known as a turning point, limit point or fold, arises when two steady states appear spontaneously as a parameter increases [34].